



# Supplement of

# Water property variability into a semi-enclosed sea dominated by dynamics, modulated by properties

Becca Beutel et al.

Correspondence to: Becca Beutel (rbeutel@student.ubc.ca)

The copyright of individual parts of the supplement might differ from the article licence.

#### **Contents**

- S1 Model Evaluation
- S2 Sensitivity Analysis
- 10 S3 Loop Water
  - S4 Attribution Calculation
  - S5 Additional Supporting Figures
  - Figures S1-S12

## S1 Model Evaluation

25

35

Tracer evaluations were conducted using publicly available datasets of salinity as absolute salinity (S<sub>A</sub>), temperature as conservative temperature (θ), DO, NO<sub>3</sub>, NH<sub>4</sub>, TA, and DIC from CTD and bottle measurements (Department of Fisheries and Oceans Canada, 2024a, b, c; Jiang et al., 2021; Miller et al., 2013; Risien et al., 2022), these datasets are summarized in table A1 but the data used in evaluations was kept on hourly timescales to match the model resolution. It should be noted that not all datasets within table A1 were used in the evaluations (e.g. GEOTRACES data) due limited overlap with the LiveOcean domain; however, the greatest loss in observations compared to those shown in figure 1 is due to the ten year time-period of analysis. With the exception of NH<sub>4</sub>, model tracers generally matched observations well, achieving WSSs >= 0.90 over the domain. The low WSSs of NH<sub>4</sub> led to its exclusion from particle tracking simulations. The bias (RMSE) of the remaining tracers were: salinity -0.3 (0.6) g kg<sup>-1</sup>, temperature 1.0 (0.7)° C, DO -5.2 (31.3) mmol m<sup>-3</sup>, NO<sub>3</sub> 12.2 (7.2) mmol m<sup>-3</sup>, TA 87.9 (46.7) mmol m<sup>-3</sup>, and DIC 145.6 (87.1) mmol m<sup>-3</sup>.

To assess the spatial variability in model accuracy relevant to the water source divisions in this study, observations were divided into six regions (table 1): offshore surface, offshore deep, north, south, and CUC (Fig. S1), with the "domain" region added to encompass the area within Ariane boundaries (Fig. 1). While evaluations of LiveOcean's performance in the Salish Sea are beyond the scope of this paper, extensive evaluations are available in MacCready et al. (2021) and Xiong et al. (2024).

It was expected that model variability would be equal to or smaller than observed variability (normalized standard deviation <1), and this was largely true, except for TA and DIC in the northern region, which exhibit normalized standard deviations > 1.4 (Fig. S1). This anomaly may result from the limited number of observations (n = 9) available for comparison. Correlations between model variables and observations are relatively strong (>0.6) across all regions. Deep waters (offshore deep and CUC) consistently have the highest correlation with observations, whereas lower correlations were observed for DO in offshore surface waters and for TA in the domain and offshore surface waters.

Biases vary significantly by regions and tracers. Deep waters (offshore deep and CUC) generally have lower biases compared to shallow waters (offshore surface, south, north). In the case of  $\theta$ ,  $S_A$ , DIC, and TA the maximum regional bias is small, a factor of 0.02 (0.03), 0.006 (0.09), 0.02 (0.3), and 0.01 (0.2) of the mean (standard deviation), respectively. There is a more significant difference in DO and  $NO_3$ , with maximum biases up to a factor of 0.1 (0.1), and 0.2 (0.4) of the tracer mean (standard deviation), respectively. The majority of regions underestimate DO content, a known LiveOcean bias (MacCready

et al., 2021), with offshore surface and south water having the largest negative biases at -11 mmol m<sup>-3</sup> compared to the 0-380 mmol m<sup>-3</sup> range in these regions. Unlike the other regions, DO is overestimated in the north (again by 11 mmol m<sup>-3</sup>). All regions overestimate NO<sub>3</sub> (by at least 2 mmol m<sup>-3</sup>), by up to 5.1 mmol m<sup>-3</sup> in the offshore surface and south waters, a potentially significant amount of the 0-39 mmol m<sup>-3</sup> range in these regions.

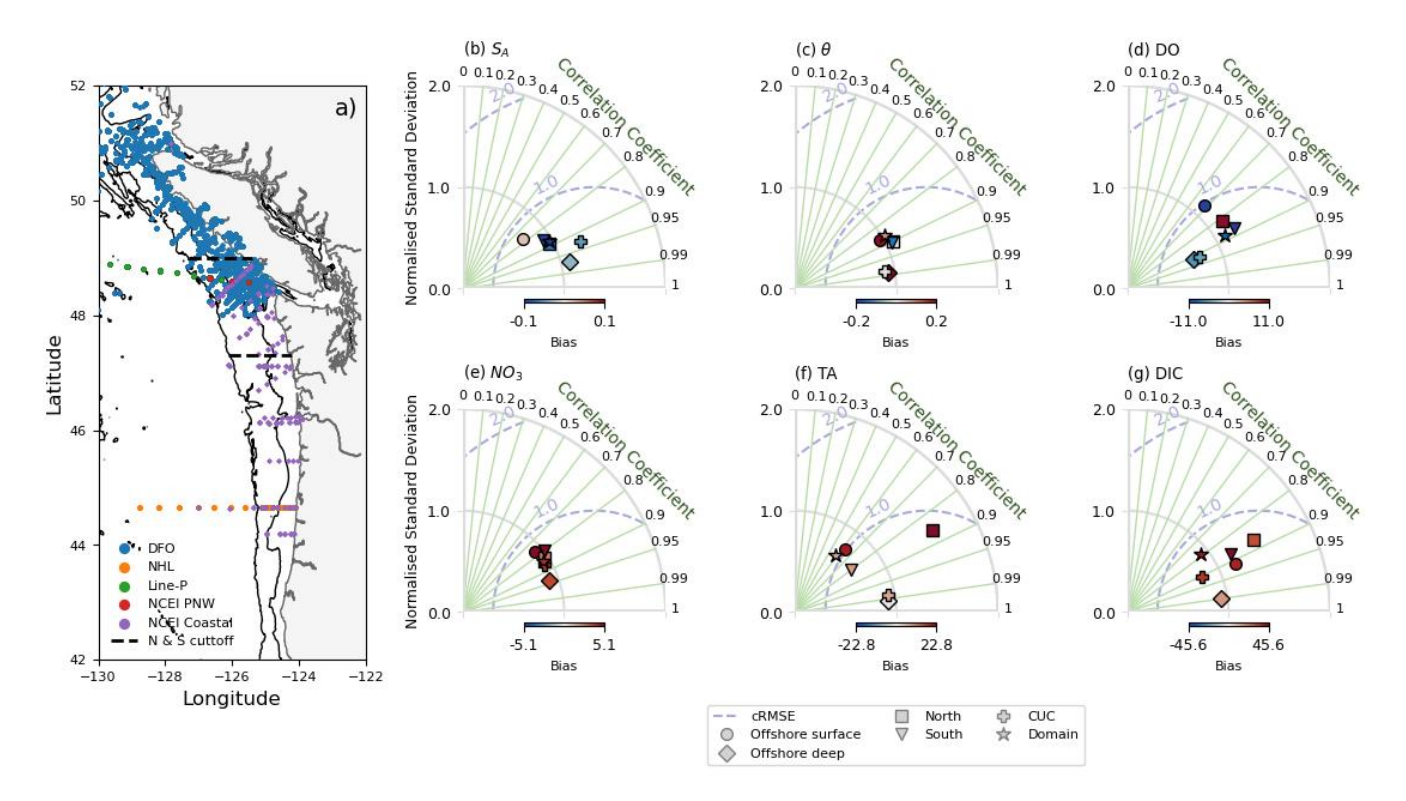


**Figure S1.** Map (a) of observations used for the LiveOcean evaluations in this study coloured by the data source. Dashed black lines signify the north and south cutoff, and 200 m and 2000 m isobaths in black signify the shelf, slope, and offshore divisions, as in table 1. Taylor diagrams (b-g) of LiveOcean absolute salinity (b), conservative temperature (c), DO (d), NO<sub>3</sub> (e), TA (f), and DIC (g) compared to observations. Each region is differentiated based on their corresponding marker symbol. Normalized standard deviation is represented by the distance from horizontal and vertical axes, with regions closest to 1 having the closest match to observed spatial and temporal variability; correlation (based on Pearson's r) is shown on the radial axis, with regions closer to 1 having better agreement with observations than those closer to 0; the centred root mean square error (cRMSE) is represented by dashed curves within each plot, with lower cRMSE indicating a better match; bias is represented by a diverging colourbar for each subplot, colours closest to white indicate the lowest bias, red indicates an overestimation by the model, and blue an underestimation.

#### **S2 Sensitivity Analysis**

## 45 S2.1 South waters

The water sources along the southern analysis boundary are defined based on their salinity. An estimate of a  $33.5\,\mathrm{g\,kg^{-1}}$  division between south shelf water and CUC in the model was chosen based on the location of flow cores at the southern boundary (Fig. S2a and e): the core of CUC transport is located between 200-275 m (Pierce et al., 2000) during downwelling (Fig. S2b) and upwelling (Fig. S2f), and the south shelf water limited to the depth of the shelf break. Increasing the salinity division to  $33.7\,\mathrm{g\,kg^{-1}}$  deepens the core of CUC flow by about 50 m and leads to significant amount of south shelf water

below the shelf break. Decreasing the division to  $33.3\,\mathrm{g\,kg^{-1}}$  moves the core of CUC flow to the shelf region and increases the contribution of CUC water during downwelling. CUC and south shelf transport magnitudes are sensitive to the choice of salinity division (Fig. S2), in particular during downwelling (Fig. S2). However, the alignment of the CUC and shelf water flow cores with their expected location (Pierce et al., 2000; Thomson and Krassovski, 2010; Huyer et al., 1998), and LiveOcean's skill at reproducing the CUC (MacCready et al., 2021) makes the choice of salinity robust despite its sensitivity to relatively small changes in definition.

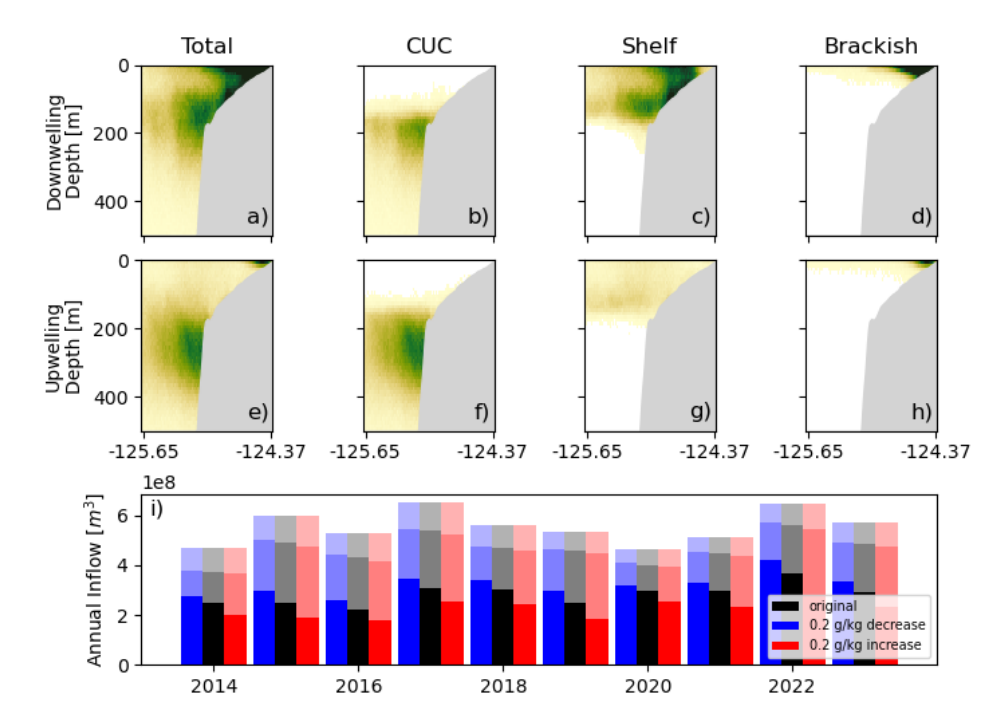


Figure S2. Water parcels crossing the southern boundary during periods of downwelling (a,b,c,d) and upwelling (e,f,g,h) and split into the CUC (b,f), south shelf water (c,g), and south brackish water (d,h) according to  $33.5\,\mathrm{g\,kg^{-1}}$  and  $32\,\mathrm{g\,kg^{-1}}$  salinity division (table 1). Darker colouring represents more transport originating from that region. Figure (i) shows the transport from the CUC (bottom, darkest portion of each bar), south shelf (middle, lighter portion), and south brackish (top, lightest portion) water source over each analysis year, and how they vary according to the different choices of depth division:  $-0.2\,\mathrm{g\,kg^{-1}}$  (blue), the divisions used in this paper (black), and  $+0.2\,\mathrm{g\,kg^{-1}}$  (red). Note that the upper and lower salinity divisions are completely independent (ie. brackish water is not impacted by the  $33.5\,\mathrm{g\,kg^{-1}}$  and CUC water is not impacted by the  $32\,\mathrm{g\,kg^{-1}}$  division.

The south shelf water and brackish water from the south are separated based on a salinity of  $32\,\mathrm{g\,kg^{-1}}$ . This choice of salinity limits the brackish source to surface water directly adjacent to the coast (Figs. S2d,h), as opposed to brackish water that has undergone mixing with shelf water as Columbia River water does very little mixing with surrounding shelf water before reaching JdF (Giddings and MacCready, 2017; Hickey et al., 2009; Thomson et al., 2007). The increase in salinity to  $32.2\,\mathrm{g\,kg^{-1}}$  has the larger impact, amounting to an average shift of 4 mSv from south shelf water to brackish water, which on average contribute 37 mSv and 27 mSv, respectively using the  $32\,\mathrm{g\,kg^{-1}}$  division.

For the observations, a salinity division of  $33.7\,\mathrm{g\,kg^{-1}}$  for the CUC and south shelf water, and  $31.5\,\mathrm{g\,kg^{-1}}$  for south brackish and south shelf water was chosen based on property-salinity diagrams of southern measurements (Fig. S3). The distinction between the CUC and south shelf water is particularly obvious in nitrate-salinity space (Fig. S3), with high nutrient and low nutrient water sources separable by salinity. This division results in a CUC with mean salinity similar to previously reported values,  $34.0\pm0.2\,\mathrm{g\,kg^{-1}}$  in this study and  $33.9\,\mathrm{g\,kg^{-1}}$  in Huyer et al. (1998). Changes to this salinity division  $(\pm0.2\,\mathrm{g\,kg^{-1}})$ 

have a minimal impact on the mean properties or the CUC, south shelf, or south brackish water (Fig. S3a-o). Most significant is the increased range of DO and  $NO_3$  in the CUC and south shelf waters in response to an increase in division to  $33.9 \,\mathrm{g\,kg^{-1}}$ , which cuts into the high salinity core of the CUC (Fig. S3r and q); however, the mean and range in  $NO_3$  and DO in these water sources remains relatively unchanged (Fig. S3a-j).

The impact of the brackish and shelf division was set to avoid the region of high DO and intermediate salinity (Fig. S3), and to capture that the temperature and DO remain the same for a large range of salinities. Changing this division by  $\pm 0.2 \,\mathrm{g\,kg^{-1}}$  has very little impact on the mean and range in properties of either the south shelf or brackish water (Fig. S3).

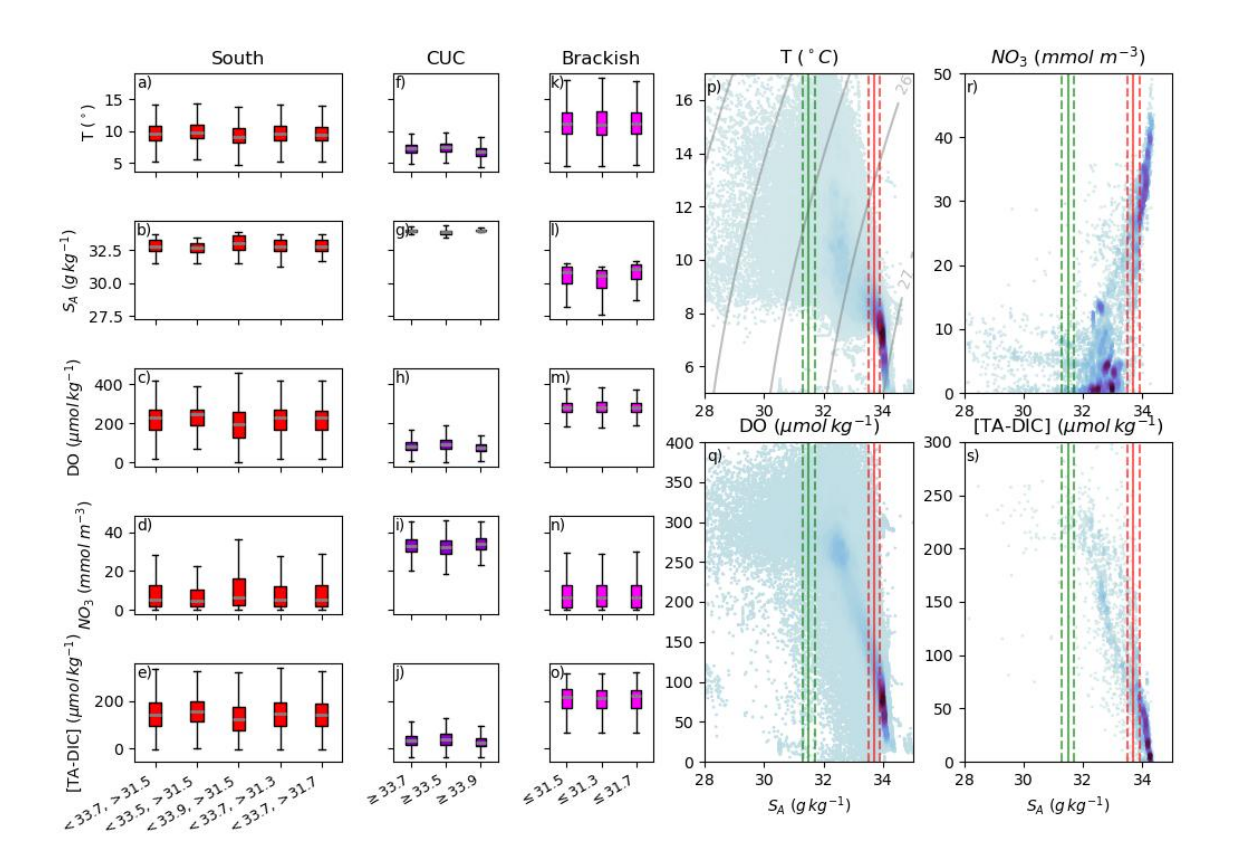
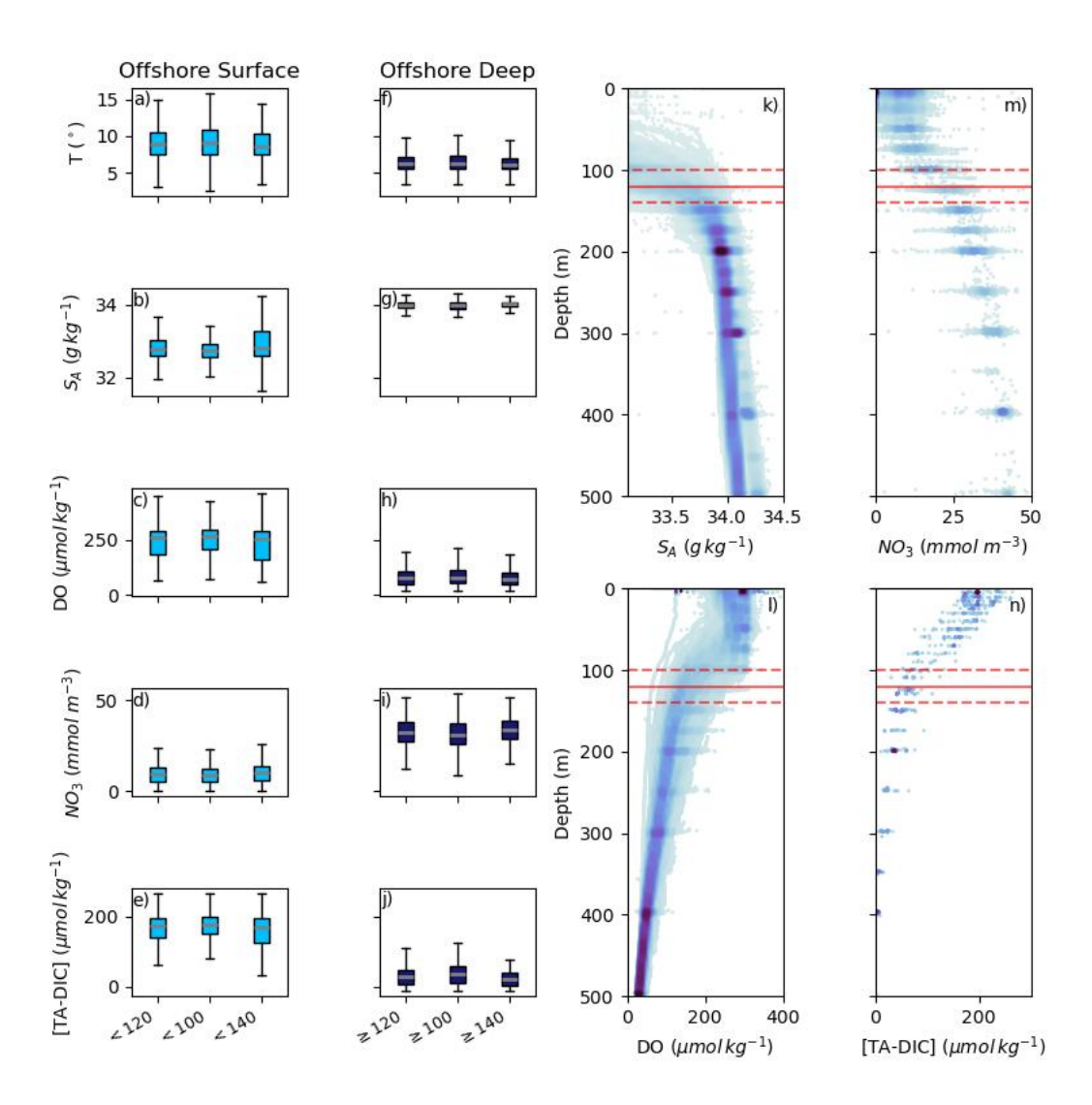


Figure S3. Box plots (a-o) of observed water source property ranges and their response to changes in the salinity division, the leftmost box in each plot is the range in properties reported in this paper. The box plots highlight that property ranges in each source water change little according to a  $\pm 0.2 \,\mathrm{g\,kg^{-1}}$  change in salinity cutoff. Property-property diagrams of T-S<sub>A</sub> (p), DO-S<sub>A</sub> (q), NO<sub>3</sub>-S<sub>A</sub> (r), and [TA-DIC]-S<sub>A</sub> (s) show the locations of water source cores (darker colour represent a higher density of parcels) relative to lower and upper salinity cutoffs (green and red solid lines, respectively) and the tested buffers (dashes lines).

# 75 S2.2 Offshore Waters

The definition of two offshore water sources originated in the analysis of nutrient observations (Fig. S4), offshore observations tended to either have high nutrient concentrations, or concentrations near zero. A depth division of 120 m effectively separated the two water sources, water shallower than 120 m corresponded to the low nutrient water, where nutrients were consumed by photosynthesis in the shallower layer (Cummins and Ross, 2020; Li et al., 2005). Comparing this 120 m to divisions 20 m



**Figure S4.** Box plots (a-j) of observed water source property ranges and their response to changes in the depth division. The leftmost box in each plot is the range in properties reported in this paper, ranges change little according to a  $\pm 20$  m change in depth cutoff. Property-depth diagrams of  $S_A$  (k), DO (l), NO<sub>3</sub> (m), and [TA-DIC] (n) show the locations of water source cores (darker colour represent a higher density of parcels) relative to the 120 m depth cutoff (red solid line) and the tested buffers (dashes red lines).

This same depth division was tested in the modelled results (Fig. S5), like in the observations a distinct high nutrient core emerges (darker colours in figure S5e). Using the 120 m cutoff discerned from observations, the core of high nutrient water is completely encompassed in deep water (shades of red in figure S5f). Conversely, a deeper, 140 m, depth division leads to a split in the high nutrient core between deep and shallow water (Fig. S5g). The distinction between a 120 m and 100 m cutoff (Fig. S5h) is less clear, the 100 m cutoff simply means that more low-nutrient water is encompassed in the deep water source. The impact of the depth division is small relative to the total contribution of offshore water; a change from a 120 m to 100 m leads to a mean shift (from shallow to deep water) of 3 mSv compared to the mean 49 mSv contribution from offshore water. Changes in the mean NO<sub>3</sub> concentration, and in other tracers, are more noticeable in the offshore surface water due to the fewer water parcels originating from this water source. Despite the up to 3.6 mmol m<sup>-3</sup> shift in mean NO<sub>3</sub>, the offshore deep and shallow water sources remain distinct from one another and interannual and seasonal variability has the same signal. A deepening of the depth division to 140 m makes the offshore surface water more similar to the north and south shelf water sources by increasing the NO<sub>3</sub> concentration and decreasing the DO content (not shown), while the 100 m depth division makes the properties of those water sources diverge more. As offshore surface, north, and south water were expected to have relatively similar properties (Fig. 6), and the 140 m depth division cuts into the high nutrient core (Fig. S5g), we believe that the 120 m represents the best depth to distinguish the offshore water sources.

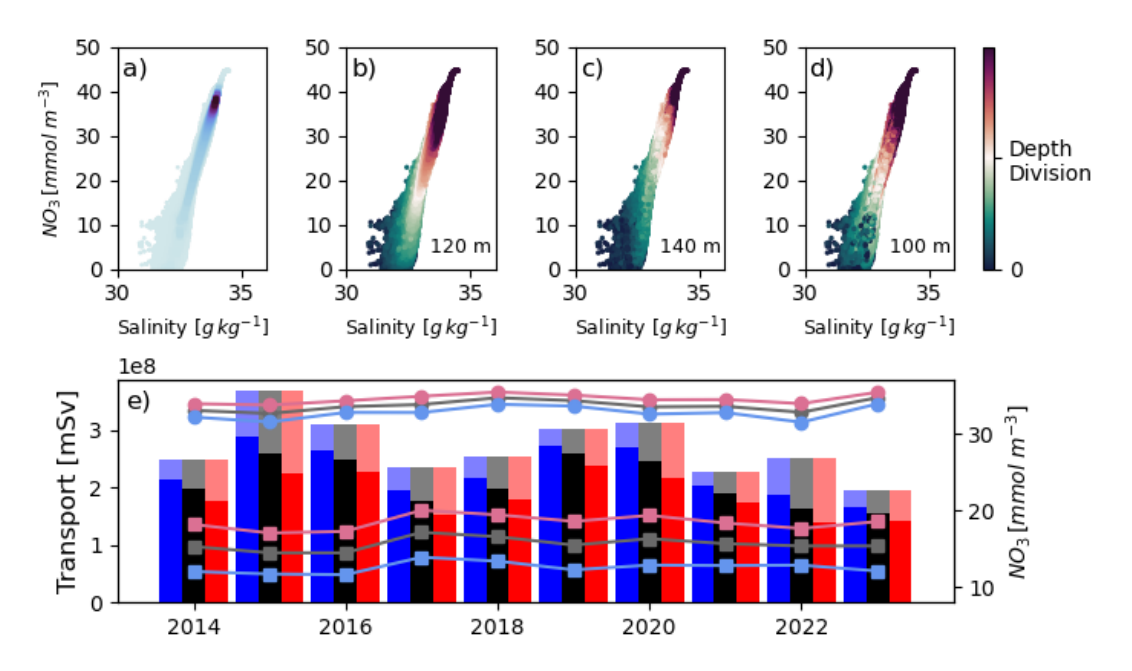
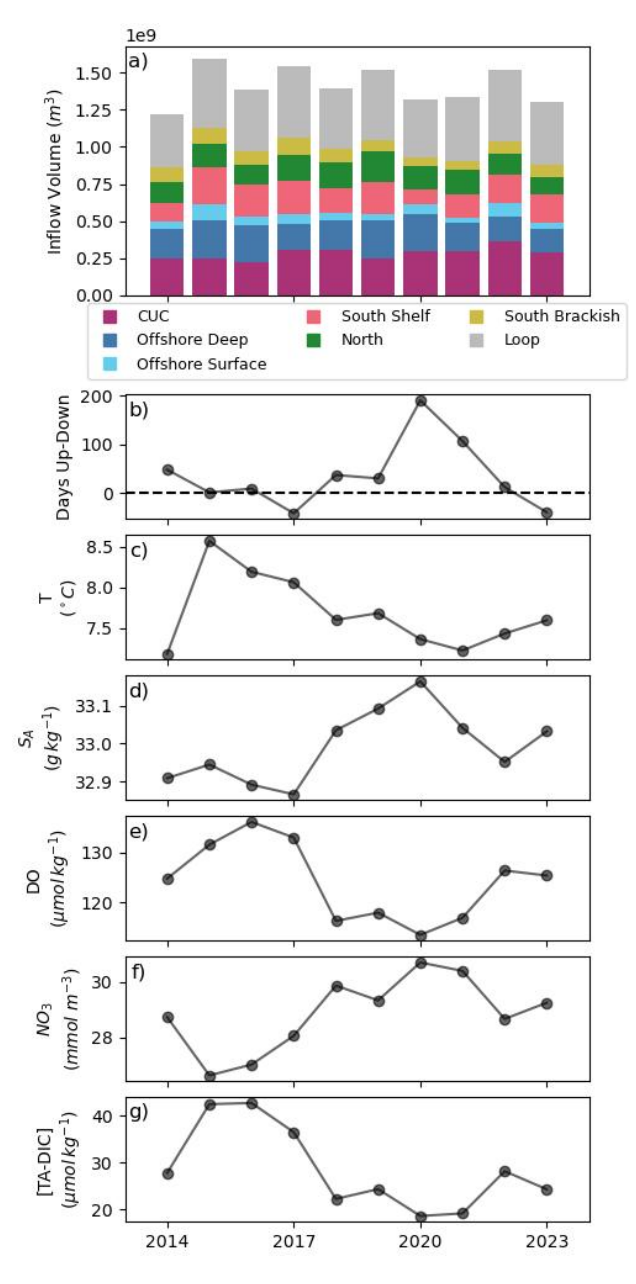


Figure S5. Offshore water parcels in  $NO_3 - S_A$  space (a,b,c,d). Shades of light blue to dark purple in (a) represent the number of parcels with a given salinity and  $NO_3$  concentration, darker shades indicate more parcels. Figures (b)-(d) are coloured by depth, shades of green indicate parcels shallower than the depth division (120 m, 140 m, or 100 m - provided at the bottom right corner of each figure), and shades of red indicate parcels deeper than it. Figure (e) shows the transport (bars) and average  $NO_3$  (line) from the offshore deep (darker portion of each bar, higher  $NO_3$  lines with round marker) and shallow (the lighter portion of each bar, lower lines with square marker) water sources over each analysis year and how they vary according to the different choices of depth division: 100 m (blue), 120 m (black), 140 m (red).

#### S3 Loop Water

Loop water, JdF outflow that crossed back over the initialization section more than 24 hours after seeding, is the largest single source of JdF inflow. Its annual contribution to annual flow and property variability are summarized in figures S6 and S7. As noted in the main text, this reflux flow is made up of an unknown mixture of the Pacific sources and of river discharge

originating in the Salish Sea. Thus, it is strongly influenced by the contribution of the Pacific Sources and cannot be easily separated from them as a unique contributor to variability.



**Figure S6.** (a) Volume from the CUC (purple), offshore deep (navy), offshore surface (light blue), north (green), south (red), brackish (pink), and loop (grey) water into the Salish Sea over one year (combined periods of downwelling, spring transition, upwelling, and fall transition). (b) Difference in the length of upwelling and downwelling in each year.

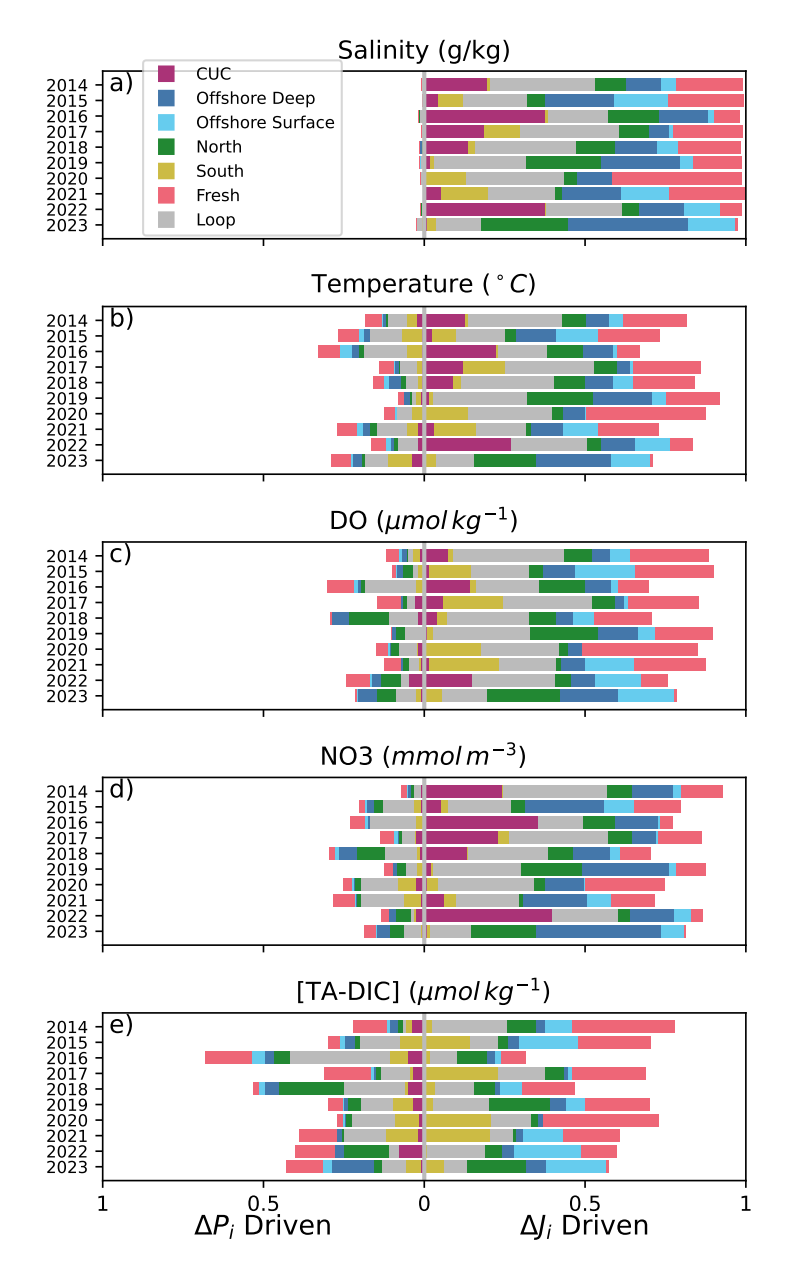


**Figure S7.** Attribution of changes in Salish Sea inflow flux of salinity (a), temperature (b), DO (c), NO<sub>3</sub> (d), and [TA-DIC] (e) to interannual differences in water source inflow volumes (right or side of the graph) or to interannual differences in water source properties (left side).

## **S4** Attribution Calculation

Additional steps for the calculation of equation 2 from equation 1 are provided below.

110 
$$PJ = \sum P_i J_i$$

Using a finite difference approach we can take the change (over time, over density bins, etc.) from base P and J values:

$$P^{base}J^{base} + \Delta(PJ) = \sum (P_i^{base} + \Delta P_i)(J_i^{base} + \Delta J_i)$$

Solving for  $\Delta(PJ)$ :

$$\Delta(PJ) = \sum [(P_i^{base} + \Delta P_i)(J_i^{base} + \Delta J_i) - P_i^{base}J_i^{base}]$$

$$= \sum [P_i^{base}J_i^{base} + P_i^{base}\Delta J_i + \Delta P_iJ_i^{base} + \Delta P_i\Delta J_i - P_i^{base}J_i^{base}]$$

 $P_i^{base}J_i^{base}$  is constant for each water source so can be cancelled out, which brings us to equation 2:

$$\Delta(PJ) = \sum [P_i^{base} \Delta J_i + \Delta P_i J_i^{base} + \Delta P_i \Delta J_i]$$

# **S5 Additional Supporting Figures**

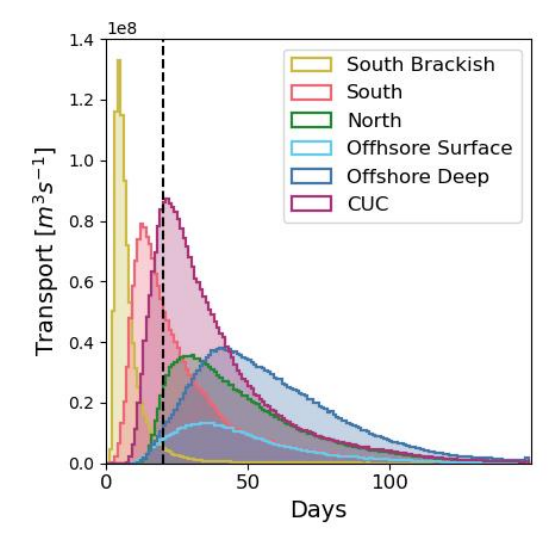


**Figure S8.** Parcel age at the time of boundary crossing, weighted by transport. Parcels in the offshore water masses in particular exceed the minimum upwelling-downwelling buffer time of twenty days (dashed black line) meaning that many of their trajectories could have been impacted by a preceding period.

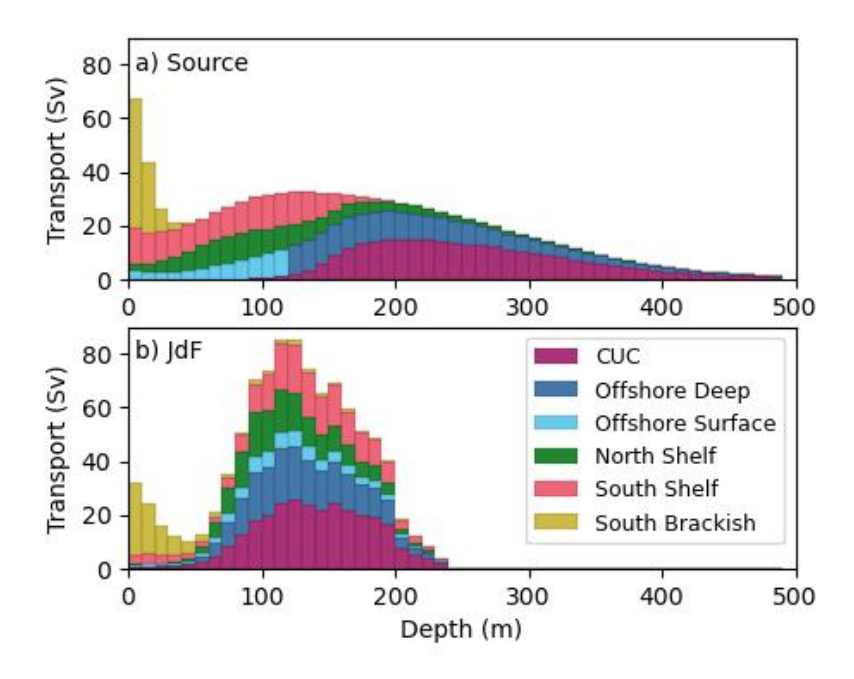
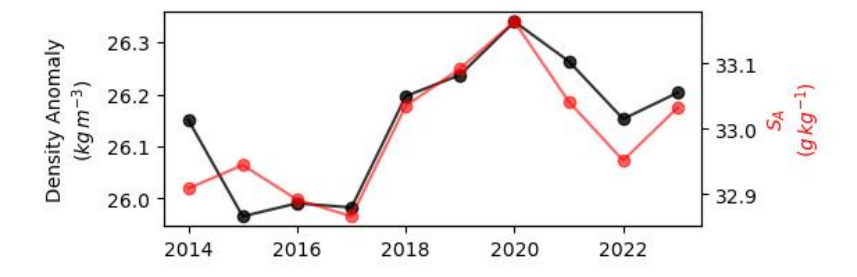
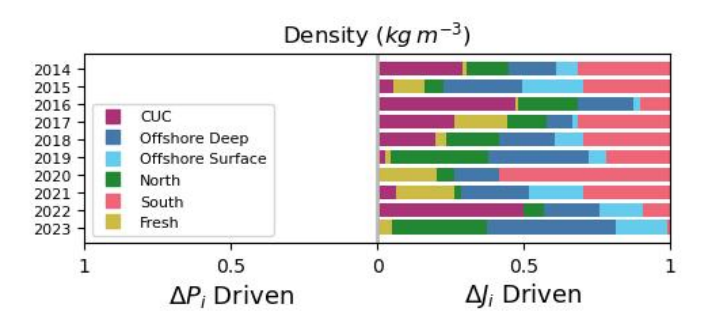


Figure S9. Histograms of transport weighted parcel depth at their location of origin (a) or at the initialization transect (b).



**Figure S10.** Mean transport weighed annual density anomaly (black) and salinity (red) of Salish Sea inflow. The interannual variability of these two properties are well correlated (r=0.9, p=0.001).



**Figure S11.** Attribution of changes in Salish Sea inflow density to interannual differences in water source inflow volumes (right or side of the graph) or to interannual differences in water source properties (left side). Property driven variability in density is not zero, just too small to appear in this figure.

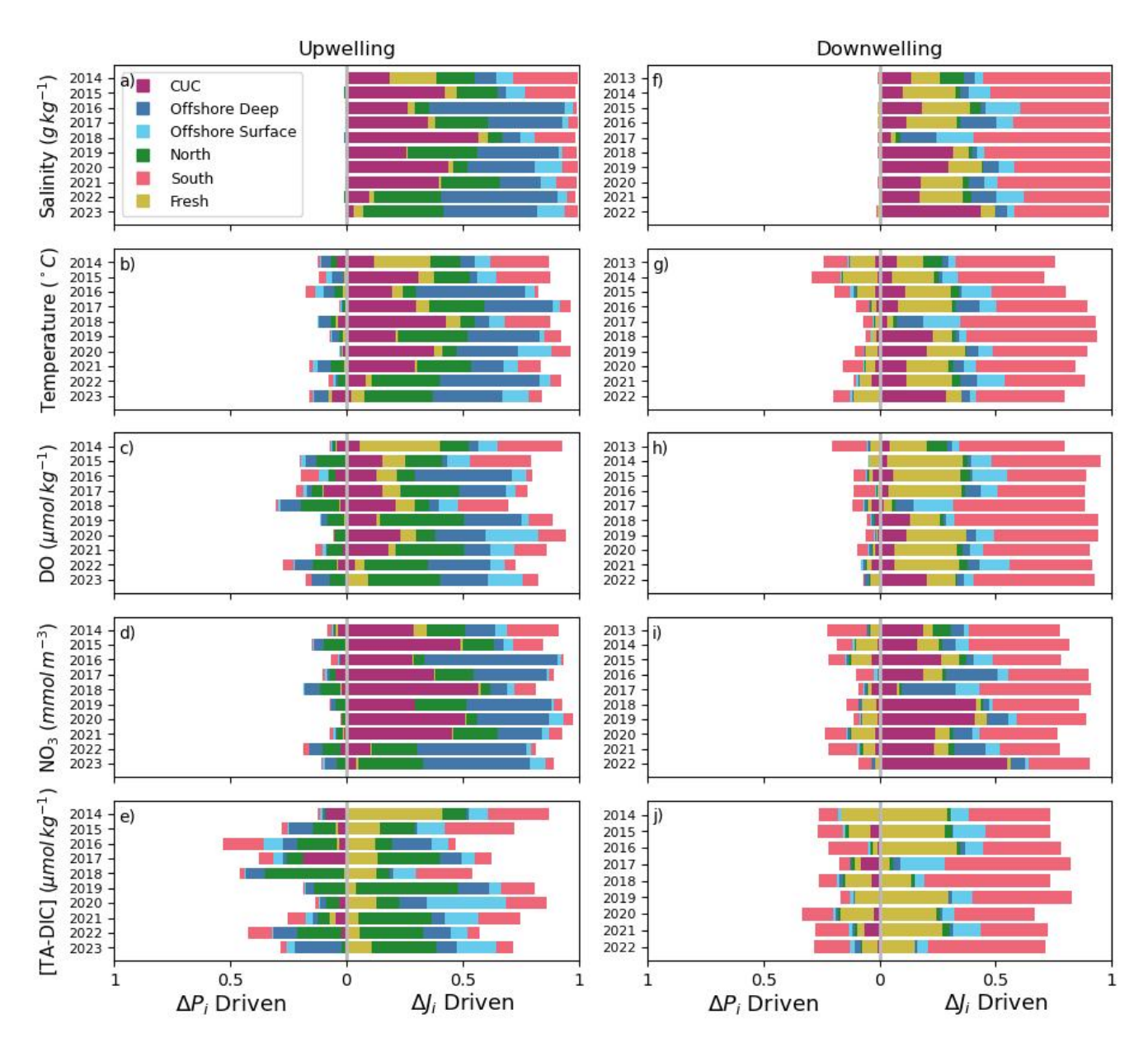


**Figure S12.** Seasonal (upwelling in the left column, downwelling in the right) attribution of changes in Salish Sea inflow flux of salinity (a,f), temperature (b,g), DO (c,h), NO<sub>3</sub> (d,i), and [TA-DIC] (e,j) to interannual differences in water source inflow volumes (right or side of the graph) or to interannual differences in water source properties (left side).

#### 120 References

130

145

150

- Cummins, P. F. and Ross, T.: Secular trends in water properties at Station P in the northeast Pacific: An updated analysis, Progress in Oceanography, 186, 102 329, https://doi.org/10.1016/j.pocean.2020.102329, 2020.
- Department of Fisheries and Oceans Canada: IOS Rosette Bottle Data, https://data.cioospacific.ca/erddap/tabledap/IOS\_BOT\_Profiles.html, 2024a.
- 125 Department of Fisheries and Oceans Canada: The GEOTRACES Intermediate Data Product 2021v2 (IDP2021v2), https://data.cioospacific.ca/erddap/tabledap/IOS CTD Profiles.html, 2024b.
  - Department of Fisheries and Oceans Canada: IOS Moored CTD Data, https://data.cioospacific.ca/erddap/tabledap/IOS\_CTD\_Moorings. html, 2024c.
  - Giddings, S. N. and MacCready, P.: Reverse Estuarine Circulation Due to Local and Remote Wind Forcing, Enhanced by the Presence of Along-Coast Estuaries, Journal of Geophysical Research: Oceans, 122, 10184–10205, https://doi.org/10.1002/2016JC012479, 2017.
  - Hickey, B., McCabe, R., Geier, S., Dever, E., and Kachel, N.: Three interacting freshwater plumes in the northern California Current System, Journal of Geophysical Research: Oceans, 114, 2008JC004 907, https://doi.org/10.1029/2008JC004907, 2009.
  - Huyer, A., Barth, J., Kosro, P., Shearman, R., and Smith, R.: Upper-ocean water mass characteristics of the California current, Summer 1993, Deep Sea Research Part II: Topical Studies in Oceanography, 45, 1411–1442, https://doi.org/10.1016/S0967-0645(98)80002-7, 1998.
- Jiang, L.-Q., Feely, R. A., Wanninkhof, R., Greeley, D., Barbero, L., Alin, S. R., Carter, B. R., Pierrot, D., Featherstone, C., Hooper, J., Melrose, D. C., Monacci, N. M., Sharp, J. D., Shellito, S. M., Xu, Y.-Y., Kozyr, A., Byrne, R. H., Cai, W.-J., Cross, J. N., Johnson, G. C., Hales, B., Langdon, C., Mathis, J. T., Salisbury, J. E., and Townsend, D. W.: A compiled data product of profile, discrete biogeochemical measurements from 35 individual cruise data sets collected from a variety of ships in the southern Salish Sea and northern California Current System (Washington state marine waters) from 2008-02-04 to 2018-10-19, https://www.ncei.noaa.gov/data/oceans/ncei/ocads/metadata/0219960.htmll, https://doi.org/10.25921/531n-c230, 2021.
  - Li, M., Myers, P. G., and Freeland, H.: An examination of historical mixed layer depths along Line P in the Gulf of Alaska, Geophysical Research Letters, 32, 2004GL021911, https://doi.org/10.1029/2004GL021911, 2005.
  - MacCready, P., McCabe, R. M., Siedlecki, S. A., Lorenz, M., Giddings, S. N., Bos, J., Albertson, S., Banas, N. S., and Garnier, S.: Estuarine Circulation, Mixing, and Residence Times in the Salish Sea, Journal of Geophysical Research: Oceans, 126, https://doi.org/10.1029/2020JC016738, 2021.
  - Miller, L. A., Christian, J. R., Davelaar, M., Johnson, W. K., and Joe Linguanti, J.: Dissolved inorganic carbon (DIC), pH on total scale, total alkalinity, water temperature, salinity and other variables collected from discrete sample and profile observations during the R/Vs Endeavour, CCGS John P. Tully and Parizeau Line P cruises in the Coastal Waters of SE Alaska, Gulf of Alaska and North Pacific Ocean from 1985-02-12 to 2017-02-20 (NCEI Accession 0110260), https://www.ncei.noaa.gov/access/metadata/landing-page/bin/iso?id=gov.noaa.nodc:0110260taPackage.html, https://doi.org/https://doi.org/10.3334/cdiac/otg.clivar line p 2009, 2013.
  - Pierce, S., Smith, R., Kosro, P., Barth, J., and Wilson, C.: Continuity of the poleward undercurrent along the eastern boundary of the mid-latitude north Pacific, Deep Sea Research Part II: Topical Studies in Oceanography, 47, 811–829, https://doi.org/10.1016/S0967-0645(99)00128-9, 2000.
- Risien, C., Fewings, M., Fisher, J., Peterson, J., Morgan, C., and Peterson, W.: Spatially gridded cross-shelf hydrographic sections and monthly climatologies from shipboard survey data collected along the Newport Hydrographic Line, 1997–2021, https://doi.org/10.5281/zenodo.5814071, 2022.
  - Thomson, R., Mihály, S., and Kulikov, E.: Estuarine versus transient flow regimes in Juan de Fuca Strait, Journal of Geophysical Research, 112, https://doi.org/10.1029/2006JC003925, 2007.
- Thomson, R. E. and Krassovski, M. V.: Poleward reach of the California Undercurrent extension, Journal of Geophysical Research: Oceans, 115, https://doi.org/10.1029/2010JC006280, 2010.
  - Xiong, J., MacCready, P., and Leeson, A.: Impact of estuarine exchange flow on multi-tracer budgets in the Salish Sea, https://doi.org/10.22541/essoar.172252837.71181115/v1, 2024.